Molecular Dynamics Simulation of Dextran Extension by Constant Force in Single Molecule AFM

Igor M. Neelov, David B. Adolf, Tom C. B. McLeish, and Emanuele Paci
Interdisciplinary Research Centre in Polymer Science and Technology and School of Physics and Astronomy, University of Leeds, Leeds, United Kingdom

ABSTRACT The extension of 1–6 polysaccharides has been studied in a series of recent single molecule AFM experiments. For dextran, a key finding was the existence of a plateau in the force-extension curve at forces between 700 and 1000 pN. We studied the extension of the dextran 10-mer under constant force using atomistic simulation with various force fields. All the force fields reproduce the experimental plateau on the force-extension curve. With AMBER94 and AMBER-GLYCAM04 force fields the plateau can be explained by a transition of the glucopyranose rings in the dextran monomers from the chair ($^4C_1$) to the inverted chair ($^1C_4$) conformation while other processes occur at smaller (rotation around C5-C6 bond) or higher (chairs to boat transitions) forces. The CHARMM force field provides a different picture which associates the occurrence of the plateau to chair-boat transitions of the glucopyranose rings.

INTRODUCTION

Carbohydrates and carbohydrate-containing biopolymers play a very important role in living cells and have many potential applications in pharmaceutical industry and material science. Their high degree of structural and conformational flexibility leads to the rich conformational behavior of these polymers, including a complex elastic response under the action of an external force. There are several possible ways of linking saccharide rings in a linear polymer, for example 1–4 and 1–6 linkages (i.e., connecting C_1 and C_4 or C_1 and C_6 carbon atoms of neighboring sugar monomers). Polysaccharides with 1–6 linkage have greater flexibility and more complex conformational behavior due to the additional bond between neighboring rings.

The extension of 1–6 polysaccharides has been studied in a series of single molecule AFM experiments (1–4). A key finding for dextran was the existence of a plateau in the force-extension curve. This plateau starts at forces of 700–900 pN for native dextran and at 250–350 pN for carboxymethylated dextran. These results sparked a debate concerning the origin of this plateau. Rief et al. (1) initially attributed the plateau to a rotation around the C_5-C_6 bond (i.e., to conformational transition of $O_5C_5C_6O_6$ dihedral angle) in each monomer. Marszalek et al. (2–4) suggested that the plateau occurs due to a chair-boat transition of the glucopyranose rings during the extension of dextran chain. To interpret the experimental findings, Rief et al. (1) also performed molecular dynamics (MD) simulations of a short chain consisting of five monomers subject to a constant pulling speed. The force extension curve extracted from the simulation showed a plateau but the conformational transitions responsible for the plateau were not characterized in detail. Marszalek et al. (2) estimated the monomer extension Δd by using ab initio calculations of the dextran monomer length (i.e., the distance d between O_1 and O_6 atoms) in the chair ($d_{chair} = 4.412$ Å) and boat ($d_{boat} = 5.696$ Å) conformations of the glucopyranose ring; the resulting $\Delta d = d_{boat}$-$d_{chair} = 1.284$ Å, agrees well with their average experimental extension of dextran per monomer. In a recent article, Lee et al. (5) presented results from a CHARMM-based (6) MD simulation of dextran and pustulan, where extension was achieved by pulling the molecules at constant speed. It was found that the extension in the dextran plateau region occurs due to a chair-boat conformational transition of the glucopyranose rings.

The conformational properties of simple sugars play an important role in the structure-function relationships governing polysaccharides and glycoproteins. This has motivated many efforts to calculate the conformational structure of different monosaccharides. Different methods were used for this goal from ab initio and semiempirical calculations (7–10) to atomistic simulations. In the latter case, the AMBER (11) and CHARMM (12) force fields, originally designed for proteins and nucleic acids have been most frequently employed. In some molecular mechanics studies the MM3 force field has been used (13). Due to the conformational complexity of the carbohydrate monomers, these generic force fields give results which are not always consistent with ab initio predictions. To overcome this deficiency, several modifications of AMBER and CHARMM force fields have been designed specifically for saccharides such as united atom AMBER (14), AMBER-Homans (15), AMBER-GLYCAM (16), AMBER with GB/SA continuum model of water (17), and CHARMM-Parm22/SU01 (18). The influence of water molecules on the conformation of glucopyranose and the structure of water around monosaccharides have also been studied using quantum chemistry and force-field approaches (19,20). The quality of 20 different force fields for monosaccharides has been recently assessed (21) through a comparison of

Submitted December 6, 2005, and accepted for publication August 7, 2006.
Address reprint requests to E. Paci, Tel.: 44-113-343-3806; E-mail: e.paci@leeds.ac.uk.

0006-3495/06/11/3579/10 $2.00
doi: 10.1529/biophysj.105.079236

energies and geometries with those from ab initio and density functional methods. Principal component analysis was used for the quantitative evaluation of the force fields' quality. Even force fields specifically elaborated for carbohydrates deviate considerably from the ab initio results. Surprisingly, one of the best force fields in this review was found to be the general AMBER94 force field (22), which was not specially designed for carbohydrates.

Conformational properties of 1–4 and 1–6 linked disaccharides have also been addressed by molecular simulation. These simulations are important as they can be used as a starting point for the prediction of the structure of linear polysaccharides. For 1–6 linked disaccharides, the FF400 force field was used as early as 1980 (23). It was shown that disaccharides with a 1–6 linkage have high conformational flexibility. This was also confirmed by simulation with more recent force fields (24–26) and suggests that linear 1–6 polysaccharides should have high conformational flexibility.

The goal of this work is to identify the conformational transitions responsible for the plateau in the force-extension curve of dextran by thoroughly analyzing a large number of equilibrium simulations in a broad range of constant forces applied to dextran. Three different force fields (AMBER94, AMBER-GLYCAM04, and CHARMM) were used for this goal to moderate between the relative merits of the force fields, and to identify possible artifacts of individual force fields.

MODELS AND METHODS

Extension of linear dextran 10-mer consisting of 1–6 linked α-*d*-glucopyranose monomers (Fig. 1) was studied in the presence of a constant force applied to the ends (O1 atom of first monomer and O6 atom of last). Most calculations were done without explicit solvent. We used the PUMA package (27) with AMBER-like force fields (AMBER94 and AMBER GLYCAM04) as it was found earlier that these force fields describe the puckering behavior of glucopyranose ring better than other force fields. Some additional simulations were performed using the CHARMM program and force field (CHARMM-Parm22/SU01).

The Verlet algorithm with a time step of 1 fs was used in all simulations. The simulation length of for the dextran 10-mer was up to 1 μs at each constant force in the interval 200–2000 pN. This interval of forces corresponds to the experimental interval used in single molecule dextran extension by AFM (28). To achieve suitable local equilibration of dextran, a Brownian thermostat with a small friction coefficient (1 ps^{-1}) was used. Most simulations were performed at $T = 300$ K temperature. Simulations at high temperature ($T = 600$ K) were also performed to understand how the decrease of effective barriers for internal rotation influences the simulation results.

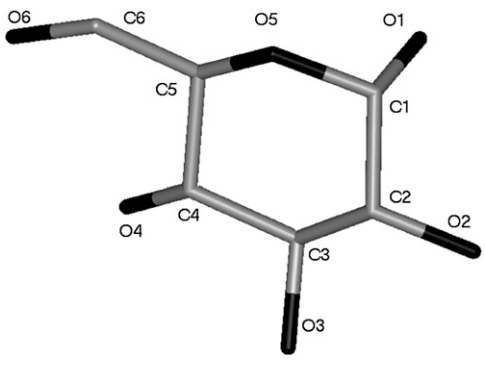

FIGURE 1 Single monomer of dextran (α-*d*-glucopyranose). Heavy atoms are indicated using standard nomenclature for saccharides. Hydrogen atoms not shown.

Simulation of a dextran 10-mer in explicit water (TIP3P) was carried out to investigate the influence of solvent on the extension mechanism and puckering behavior of the pyranose ring. In this case, the dextran was immersed in a rectangular box containing 4529 molecules of TIP3P water. Simulations were performed at constant temperature (300 K) and pressure (1 atm) using the Berendsen thermostat and barostat (29). Relatively short (20 ns) simulations were performed at three different forces ($F = 200$, 1000, and 1800 pN) to probe the main stages of dextran extension (before, during, and after the plateau region).

RESULTS AND DISCUSSION

Force-extension dependence for 10-mer

Force-extension curves for the 10-mer (where the average extension per monomer d is on the x axis and the constant force F on the y axis) are shown for the AMBER94 in Fig. 2 *A* and for AMBER-GLYCAM04 force fields in Fig. 2 *B* (*circles*). The end-to-end distance is normalized by the number of monomers in the chain to provide an easier comparison with experimental results (see Table 1). AMBER94 and AMBER-GLYCAM04 give similar results, and a plateau on the force-extension curves for both force fields is evident in both cases. The only difference between these two force fields is in the small shoulder in the force-extension curves near $F = 1500$–1800 pN (visible in Fig. 2 *A*, and not in Fig. 2 *B*). Currently available experimental data (1,2,5) suggest that this shoulder is an artifact.

To understand the molecular mechanism of dextran extension, it is important to discriminate the contributions from the extension of each of the monomers and their mutual orientation. It should be stressed that the carbohydrates' normalized end-to-end distance measured experimentally includes both these contributions. In fact, particularly at small extensions, monomers are not perfectly oriented along the direction of extension. The average monomer length was calculated as the average 10-mer contour length divided by the number of monomers. The force as a function of normalized contour length (equal to the average length of one monomer) is shown in Fig. 2 *A* and Fig. 2 *B* as triangles. At forces >600 pN (when the orientation of the monomers is strong) the difference between the two curves is small. However, at small forces the difference can be large; for example, it is 0.37 Å at $F = 200$ pN per monomer for the AMBER94 force field and 0.32 Å for the AMBER-GLYCAM04 force field. Thus the orientation of the monomers contributes to the extension of the dextran chain as a whole but only at low forces and could not contribute to the plateau of force-extension curve at higher forces (Fig. 2). The time series of the length of all the inner monomers is shown in Fig. 3. Although fluctuations are large, it appears that a discreet number of states is populated. Two states are mostly

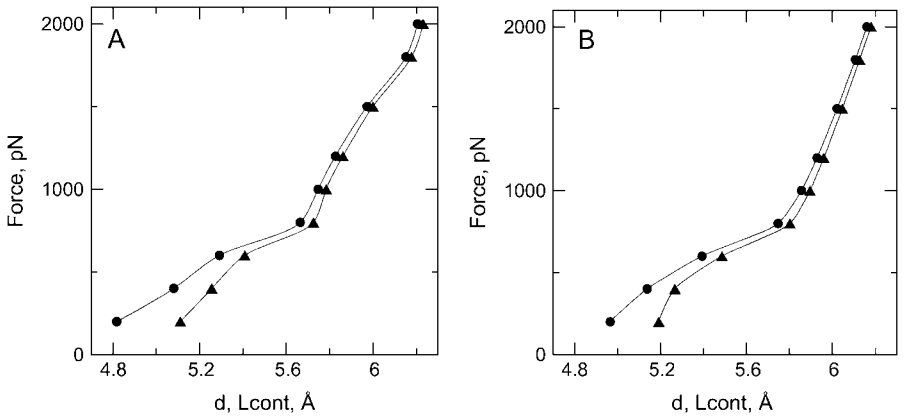

FIGURE 2 Force-extension curves for a dextran 10-mer at temperature $T = 300$ K. Circles denote the normalized average end-to-end distance, d, whereas triangles represent the normalized chain contour length, L_{cont}, for (*A*) AMBER94 and (*B*) AMBER-GLYCAM04 force fields.

populated, corresponding to a length of 5.7 and 5.9 Å, but conformations with a length of 6.1 Å are also rarely observed.

The next step is to check which processes contribute to the extension of each monomer (i.e., the increase of the O1–O6 distances of the same monomer; see *triangles* in Fig. 2) at different forces. An increase in monomer's length can be achieved through the extension of valence bonds and distortion of the valence and dihedral angles. To quantify the contribution of the first two factors to individual monomer's extension we calculated the bond lengths and selected distances between second neighboring atoms (which define valence angles) along the contour of extension (O1C1O5C5-C6O6 between O1 and O6 end atoms, see Fig. 1). We found that bond lengths along this contour extend by no more than 1.5–2% for forces $F = 700$–1000 pN. The calculations of distances between second neighboring atoms belonging to the O1C1O5C5C6O6 contour allow the contribution of the deformation of valence angles and bonds to be estimated. Such extension of bonds and the distortion of valence angles in the plateau region contribute by no more than 3–4% of the total extension of monomers and thus do not play a significant role in the overall extension.

TABLE 1 Parameters of dextran obtained from experiment and simulation

	Monomer length d (Å)	Plateau force F^* (pN)	Energy difference kcal/mol	Distance difference (Å/monomer)
Appell et al. (10)† ($F = 0$, ab initio)				
$^4C_{1(gt)}$	4.48		0	
$^4C_{1(gg)}$	5.15		0.075	
$^4C_{1(tg)}$	5.21		0.055	
$B_{14(tg)}$	5.48		8.717	
$^1C_{4(tg)}$	5.58		7.91	
$^{14}B_{(tg)}$	5.87		9.041	
Rief[1]				
($F < F^*$)		700–850	7.9	0.64
($F > F^*$)				
Fernandez et al. (33)				
($F < F^*$)	4.4	850 ± 140	11.2	1.28
($F > F^*$)	5.7			
Kawakami et al. (28) (AFM)			9.5	0.66
Lee et al. (5) (MD)				
$F < F^*$				
$^4C_{1(gt)}$	4.4			
$^4C_{1(gg,\ tg)}$	5.2–5.5			
$F > F^*$				
$T_{(tg)}$	6.30			1.1
Present (MD)				
$F < F^*$				
$^4C_{1(gg,\ tg)}$	5.2			
FF^*				
$^4C_{1(tg)}$	5.4–5.7			
$^1C_{4(tg)}$	5.7–6.0			
$F > F^*$				
$^4C_{1(tg)}$	5.9			
$^1C_{4(tg)}$	6.0			
$T_{(tg)}$	6.3			1.1

†Appell et al. (10) for energies and private communication for distances, F^* is a force in plateau region of force-extension curve.

Thus the extension of monomers must involve conformational transitions. To determine which conformational transition (i.e., a rotation around the C5C6 bond or a puckering of the glucopyranose ring) is responsible for these steplike transitions between three values of monomer length, in Fig. 3 we calculated dihedral angles that change their values in these two processes. In the first case, O5C5C6O6 and C4C5C6O6 dihedral angles were calculated at different constant forces.

The Ramachandran-like plot of $\phi 2 =$ C4C5C6O6 dihedral angle as function of $\phi 1$ (i.e., the O5C5C6O6 dihedral angle) for all the inner monomers within the 10-mer are shown in shading in Fig. 4, *A–C*, for AMBER94; in Fig. 4, *D–F*, for AMBER-GYCAM04; and in Fig. 4, *G–I*, for CHARMM. Fig. 4 *A*, *D*, and *G* are for $F = 200$ pN; the Fig. 4, *B*, *E*, and *H*, for $F = 1000$ pN; and Fig. 4, *C*, *F*, and *I*, for $F = 2000$ pN. There are three possible conformational states of O5C5C6O6 and C4C5C6O6 angles (−60°, 60°, and 180°) that correspond to the *gauche* minus ($g-$), *gauche* plus ($g+$), and *trans* (t) rotation isomers of these angles. Because angles O5C5C6O6 and C4C5C6O6 share three of four atoms there are only three possible conformational states of this pair of angles which are traditionally used for the description of

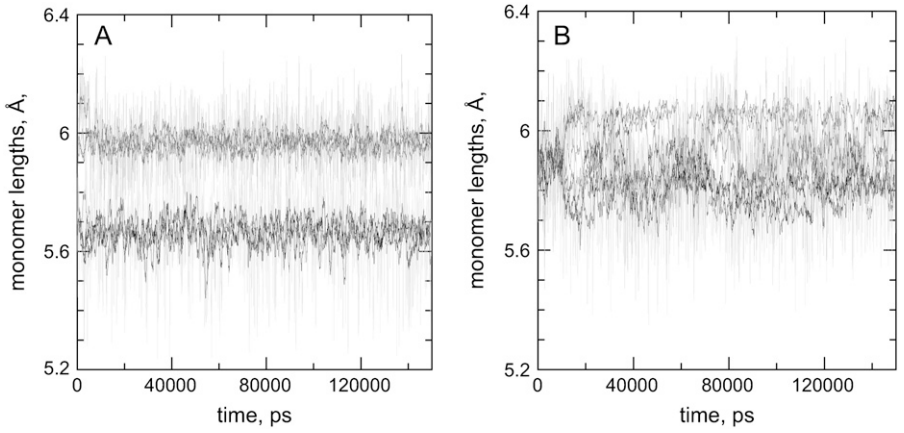

FIGURE 3 Length of the eight interior monomers (excluding first and last) in a dextran 10-mer at constant force $F = 1000$ pN and $T = 300$ K as a function of simulation time (averaged over 10-ps window). (*A*) AMBER94 and (*B*) AMBER-GLYCAM04 force fields. The length of each monomer is represented by different shade intensities.

rotation around the C5C6 bond. When the O5C5C6O6 angle is in the $g-$ state and the C4C5C6O6 is in $g+$ isomeric state, the pair of angles ($\phi1$, $\phi2$) is in the $g-g+$ state. This is the only region at force 200 pN that exists in our simulations for all force fields (*shaded dots* around ($-60°$, $60°$) in plots Fig. 4 *A*, *D*, and *G*). The second possible conformational state is $tg-$. This area is well pronounced for AMBER-like force fields (*shaded dots* around ($\phi1$, $\phi2$) = ($180°$, $-60°$) in Fig. 4, *A* and *D*) and completely absent in the case of CHARMM force field (Fig. 4 *G*). The third conformational state of this pair of angles, $g+t$, is clearly seen (but less populated than $g-g+$ and $tg-$ states) only for the AMBER94 force field (*shaded dots* near ($\phi1$, $\phi2$) = ($60°$, $-180°$) in Fig. 4 *A*) .

At the intermediate force 1000 pN (Fig. 4, *B*, *E*, and *H*) close to the end-of-plateau region in the force-extension curve (Fig. 2, *A* and *B*), the state $tg-$ becomes equally or even more populated than $g-g+$ for both AMBER-based force fields (*shaded dots* around ($\phi1$, $\phi2$) = ($180°$, $-60°$) in

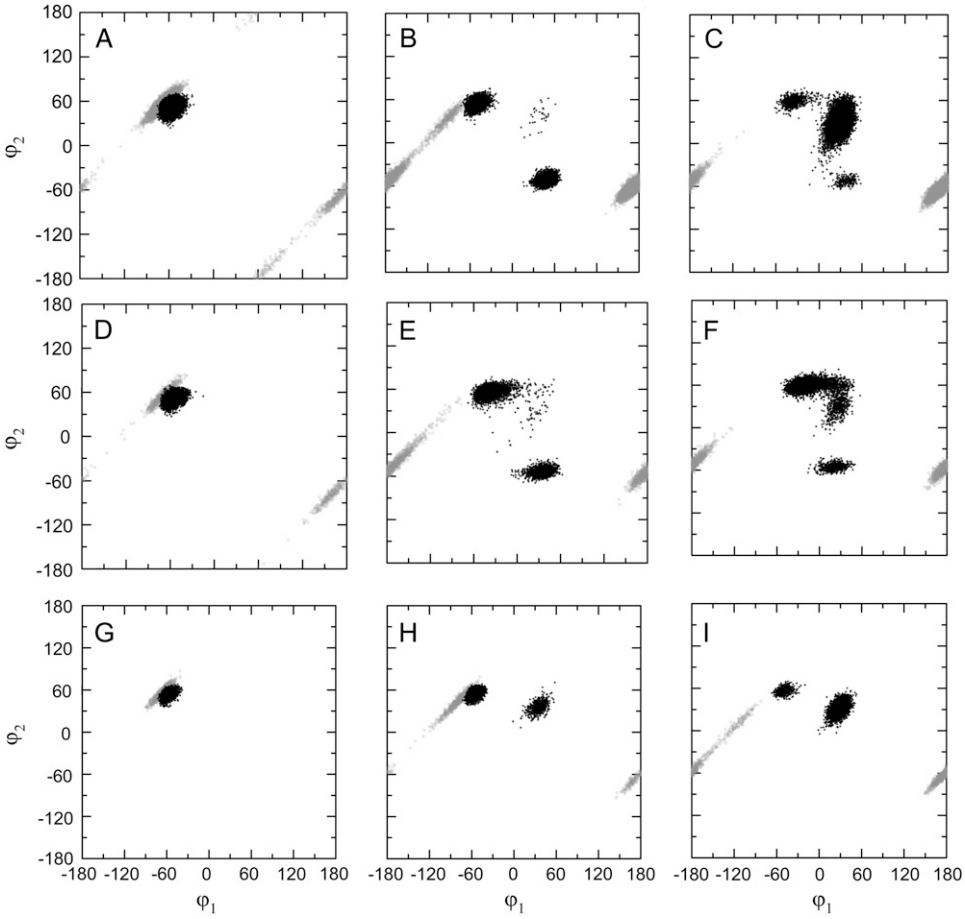

FIGURE 4 Ramachandran-like plots for two pairs of dihedral angles: first pair O5C5C6O6 ($\phi1$) and C4C5C6O6 ($\phi2$) (*shaded*), second pair C2C1O5C5($\phi1$) and C2C3C4C5($\phi2$) (*solid*) in the dextran 10-mer. (*A*) $F = 200$ pN, (*B*) $F = 1000$ pN, and (*C*) $F = 2000$ pN. Values for the eight interior dextran monomers in a 10-mer are shown. Panels *D–F*, the same as panels *A–C*, but for the AMBER-GLYCAM04 force field; and panels *G–I*, the same but for the CHARMM force field.

Fig. 4, *B* and *E*). For CHARMM at $F = 100$ pN the $tg-$ state also occurs (Fig. 4 *H*) but it is not as pronounced as for AMBER-based force fields. The state $g+t$ at this force disappear even for the AMBER94 force field (Fig. 4 *B*).

At high force $F = 2000$ pN (Fig. 4, *C*, *F*, and *I*) the state $tg-$ is the most prevalent for both the AMBER and CHARMM force fields (*shaded dots* around $(\phi1, \phi2) = (180°, -60°)$ in Fig. 4, *B*, *F*, and *I*). The state $g-g+$ (*shaded area* around $(\phi1, \phi2) = (-60°, 60°)$) completely disappears for AMBER force fields (Fig. 4, *C* and *F*) while for the CHARMM force field (Fig. 4 *I*) the $g-g+$ state ''moves'' in the direction of the $tg-$ state.

In the $g+t$ state, the monomer length is short (4.5 Å) while in the two other states ($g-g+$ and $tg-$) the monomer has nearly the same length (5.2 Å). The small population or the absence of $g+t$ state at 200 pN and greater means that the monomer is always in its longest possible state. This result is in agreement with Fig. 2's result that the length of monomer (*triangles*) at the smallest force used ($F = 200$ pN) is close to 5.2 Å. Further rotation around the C5C6 bond at higher forces could not contribute to the monomer extension and to the occurrence of the plateau region (at forces 700–100 pN).

Thus the only process that can lead to a significant extension of the monomer in the plateau region is the conformational transition of glucopyranose ring. The puckering of the glucopyranose ring can be characterized by improper dihedral angles (30). Analogous information can be obtained from pairs of dihedral angles inside the glucopyranose ring, for example, $\phi1$ = C2C1O5C5 and $\phi2$ = C2C3C4C5. The Ramachandran-like plots of the dihedral angle $\phi2$ = C2C3C4C5 as function of $\phi1$ = C2C1O5C5 are shown in Fig. 4 by solid representation for different force fields where Fig. 4, *A–C*, for AMBER94; in Fig. 4, *D–F*, for AMBER-GYCAM04; and in Fig. 4, *G–I*, for CHARMM. Fig. 4, *A*, *D*, and *G*, are for $F = 200$ pN; the Fig. 4, *B*, *E*, and *H*, for $F = 1000$ pN; and Fig. 4, *C*, *F*, and *I*, for $F = 2000$ pN. At $F = 200$ pN for all force fields (Fig. 4, *A*, *D*, and *G*), there is only one populated region of $(\phi1, \phi2) = (-60°, +60°)$ corresponding to a well-known chair conformation ($^4C_1$) of the glucopyranose ring in dextran monomers.

At $F = 1000$ pN (Fig. 4, *B*, *E*, and *H*), the chair state ($^4C_1$) is slightly displaced to $(\phi1, \phi2) = (-50°, +60°)$. At the same time, two new populated areas arise at $(\phi1, \phi2) = (50°, -60°)$ corresponding to an inverted chair ($^4C_1$) and at $(\phi1, \phi2) = (30°, 30°)$ corresponding to a boat state. The ''inverted'' chair $^1C_4$ and boat conformations of glucopyranose ring had a very small probability in the absence of force and at forces $F = 200$ pN (these conformations were absent in Fig. 4, *A*, *D*, and *G*). Application of higher forces increases the probability of the $^1C_4$ inverted chair and boat conformations. For both AMBER force fields in the plateau region ($F = 700$–1000 pN), the number of chairs in this $^1C_4$ state (size of area marked by *solid points* around $(\phi1, \phi2) = (50°, -60°)$ in Fig. 4, *B* and *E*) becomes comparable with that for $^4C_1$ state (around $(\phi1, \phi2) = (-50°, +60°)$ on the same plots). Thus the plateau on the force-extension curve could be originated by chair-inverted chair transitions (from chair $^4C_1$ to $^1C_4$ conformation).

These results contrast with those obtained using CHARMM at intermediate forces (Fig. 4 *H*). At $F = 1000$ pN, only one additional region around $(\phi1, \phi2) = (30°, 30°)$ occurs that corresponds to a boat state of glucopyranose rings in dextran 10-mer. The inverted chair conformation is completely absent (there are no points around $(\phi1, \phi2) = (50°, -60°)$ in Fig. 4 *H*). An analogous simulation at high temperature (600 K) gives for CHARMM three ensembles of conformations with angles $\phi1$ and $\phi2$ corresponding to chair ($^4C_1$, $\phi1 = -60°$ and $\phi2 = 60°$); inverted chair ($^1C_4$, $\phi1 = -60°$ and $\phi2 = 60°$); and boat ($\phi1 = 30°$ and $\phi2 = 30°$) (not shown). Thus, for CHARMM force field at high temperature, the same conformational states of the ring as for AMBER-like force fields at room temperature were obtained.

Further increase of force to $F = 2000$ pN (Fig. 4, *C* and *F*) leads to a decrease in population in both chair states for both AMBER force fields. The average absolute value of $\phi1$ = C2C1O5C5 angle decreases to near 30° (area around $(\phi1, \phi2) = (-30°, 60°)$ in the chair $^4C_1$ state and area around $(\phi1, \phi2) = (30°, -60°)$ for inverted chair $^1C_4$). For all force fields, a significant increase in the number of points in boat state (around $(\phi1, \phi2) = (30°, 30°)$) occurs. The boat state becomes dominant for AMBER94 (Fig. 4 *C*, see area around $(\phi1, \phi2) = (30°, 30°)$). This is in agreement with the occurrence of the shoulder region in Fig. 2 *A*. Thus we now can attribute this shoulder to the transitions from chair to boat conformation of glucopyranose rings for AMBER94.

This shoulder, observed only for AMBER94, is due to chair to boat transitions occurring in a small interval of forces between 1500 and 1800 pN. For AMBER-GLYCAM04, this transition occurs in a broad interval of forces and thus it is not evident in the force-extension curve. The absence of the second shoulder is in agreement with available experimental data for dextran extension (1,2,5) in single molecule AFM. The broad range of positive $(\phi1, \phi2)$ angles for boatlike states at high forces suggests that it involves more than one boatlike conformational state (e.g., boat and twisted boat conformations).

Kinetics of glucopyranose ring transitions

To get insight into the mechanism of conformational transition for the pyranose ring in plateau region of forces (700–1000 pN), the time dependence (Fig. 5) of the monomer length (Fig. 5, *A* and *B*), the diagonal lengths of glucopyranose ring (Fig. 5, *C* and *D*), and some dihedral angles (Fig. 5, *E* and *F*) for the same monomer are plotted at $F = 800$ pN .

Fig. 5 *A* shows that in the case of the AMBER94 force field, the transition is observed from a state with a monomer length $d = 5.5$–5.6 Å to a second state with $d \approx 5.8$ Å (at time near 5000 ps) and also rare transitions to a third short-lived state with $d \approx 6.0$–6.1 Å (at times near 11,000 ps and 20,000 ps).

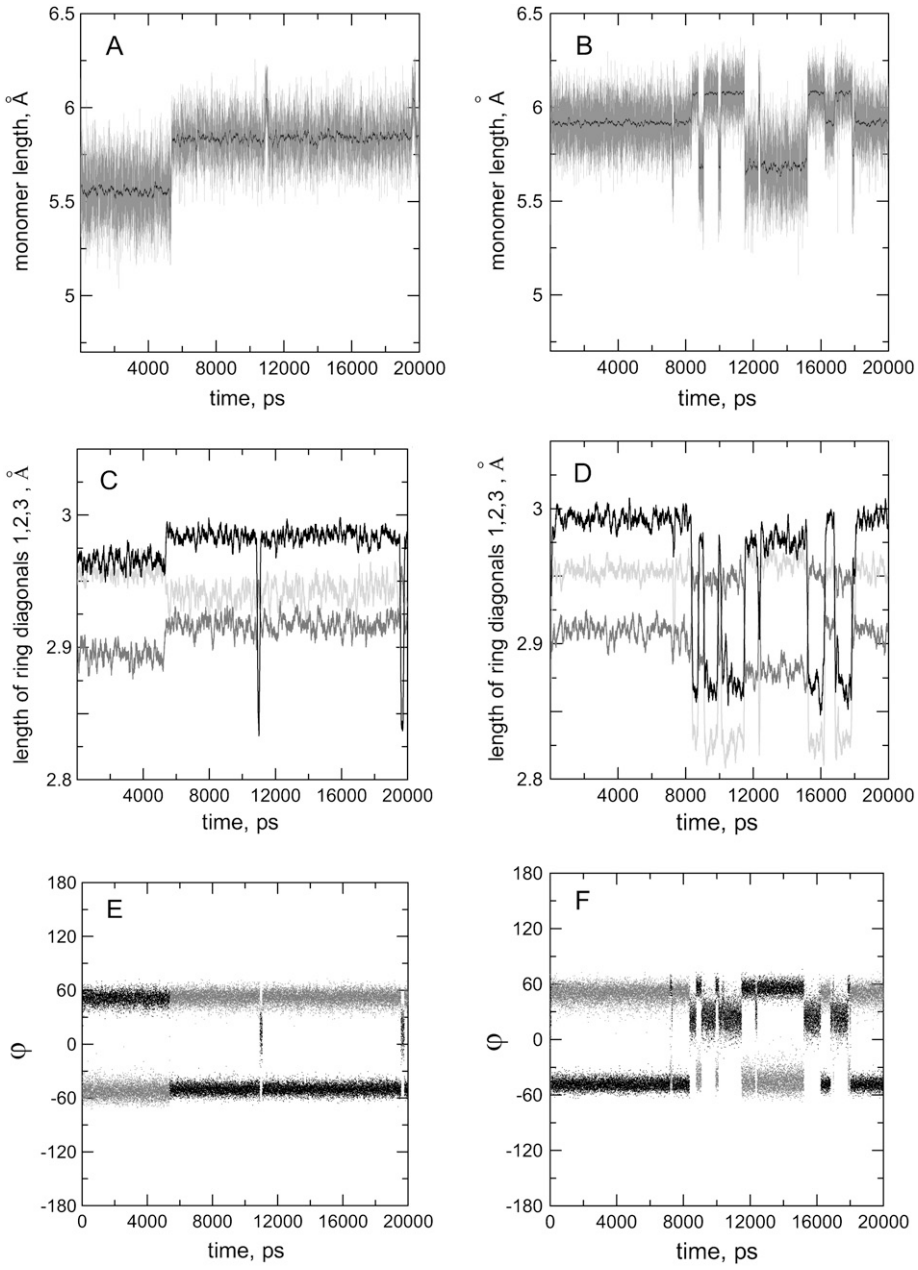

FIGURE 5 Monomer length (distance between O1 and O6 atoms) (*shaded line*) as function of time for (*A*) AMBER94 and (*B*) AMBER-GLYCAM04 force fields. The black line corresponds to data averaged over 100-ps windows. (*C*,*D*) The length of each of the three diagonals: C1–C4 (*light shaded*), C2–C5 (*solid*), and C3-O5 (*shaded*) for the dextran monomer as a function of time for (*C*) AMBER94 and (*D*) AMBER-GLYCAM04 (averaged over 100-ps window). (*E*,*F*) C2C1O5C5 (*shaded*), C2C3C4C5 dihedral angle (*solid*) of the glycopyranose ring as a function of time for AMBER94 (*E*) and AMBER-GLYCAM04 (*F*). The force is 800 pN in all cases.

Similar transitions between three states (with length of monomer d near 5.6–5.7, 5.9, and 6.1 Å) are observed at the same conditions for the AMBER-GLYCAM04 force field in Fig. 5 *B*. The starting conformational state for monomer in both force fields (in Fig. 5, *A* and *B*) was the same. The first transition from $d = 5.5$–5.6 Å to $d = 5.9$ Å in Fig. 5 *B* occurs very quickly and lines overlaps with the vertical axis in Fig. 5, *B*, *D*, and *F*.

To determine the identity of these states, reference is made to the diagonal lengths and dihedral angles. In Fig. 5, *C* and *D*, the lengths of three diagonals at $T = 300$ K are shown as a function of time. For both AMBER94 (Fig. 5 *C*) and for AMBER-GLYCAM04 (Fig. 5 *D*), the length of each diagonal fluctuates around three possible values. Transitions between these values occur at the same time as the transitions of the monomer length in Fig. 5, *A* and *B*. The lengths of the diagonals for states with $d = 5.6$–5.7 Å and 5.8–5.9 Å are close to each other and similar to those for chair and inverted chair states. The length of the diagonals of the state with largest monomer length (6.0–6.1 Å) is different and close to the length of diagonals in boat state.

In Fig. 5, *E* and *F*, the time dependences of the pairs of dihedral angles C2C1O5C5 and C2C3C4C5 for the same monomer are shown. For the chair state ($^4C_1$), they should be close to (−60°, 60°), for the inverted chair conformation ($^1C_4$) to (60°, −60°), and for the boat to (30°, 30°). At times

<5000 ps in Fig. 5 *E*, C2C1O5C5 (*shaded points*) is close to −60°, while C2C3C4C5 (*solid points*) is ~60°; i.e., the glucopyranose ring is in $^4C_1$ state. At times near 5000 ps, they interchange signs so that C2C1O5C5 is 60° and C2C3C4C5 is −60°; i.e., a transition to $^1C_4$ occurs. Exceptionally both C2C1O5C5 and C2C3C4C5 are simultaneously positive (e.g., in boat conformation at ~11,000 and 20,000 ps in Fig. 5 *E* for AMBER94 and more frequently in Fig. 5 *F* for AMBER GLYCAM04). Thus comparison of bond lengths, diagonal lengths, and dihedral angles of the same glucopyranose ring confirms that the short state corresponds to chair, the intermediate state to inverted chair, and the longest state to the boat conformation.

Ab initio results of Appell et al. (10) confirm (see Table 1) that the length of the monomer in chair conformation $^4C_1$ is minimal at ~5.2 Å, the length of the $^1C_4$ inverted chair is greater at ~5.6 Å, and the boat conformation is the longest at ~5.9 Å (see Table 1). These values are consistent with our monomer length (d = 5.6, 5.8, and 6.1 Å, correspondingly; see Table 1). The only difference is that the single monomer length obtained from molecular dynamics simulations under force is greater than ab initio values due to additional elastic deformation of the monomer.

Representative structures

In Fig. 6, *A–D*, are shown the representative structures chosen by determining the average $\phi1$ and $\phi2$ for each basin in Fig. 4 *B* and by choosing the structures with $\phi1$ and $\phi2$ angles closest to these values. Glucopyranose ring conformations in these states correspond to the chair $^4C_1$ (Fig. 6 *A*), the inverted chair $^1C_4$ (Fig. 6 *B*), and the boat/twisted boat conformations (Fig. 6 *C*) of the glucopyranose ring. The very rare inverted boat conformation (Fig. 6 *D*) is also shown for completeness.

Comparison of the probability of chair and boat states for different force fields

The number of conformations in each of the glucopyranose ring states (i.e., chair, inverted chair, boat, and inverted boat) were obtained by dividing all trajectories into four parts corresponding to each state. This division was made on the basis of signs of pair of angles $\phi1$ = C2C1O5C5 and $\phi2$ = C2C3C4C5. We suppose that

State 1: If $\phi1 \leq 0$ and $\phi2 \geq 0$, the ring is in chair conformation.

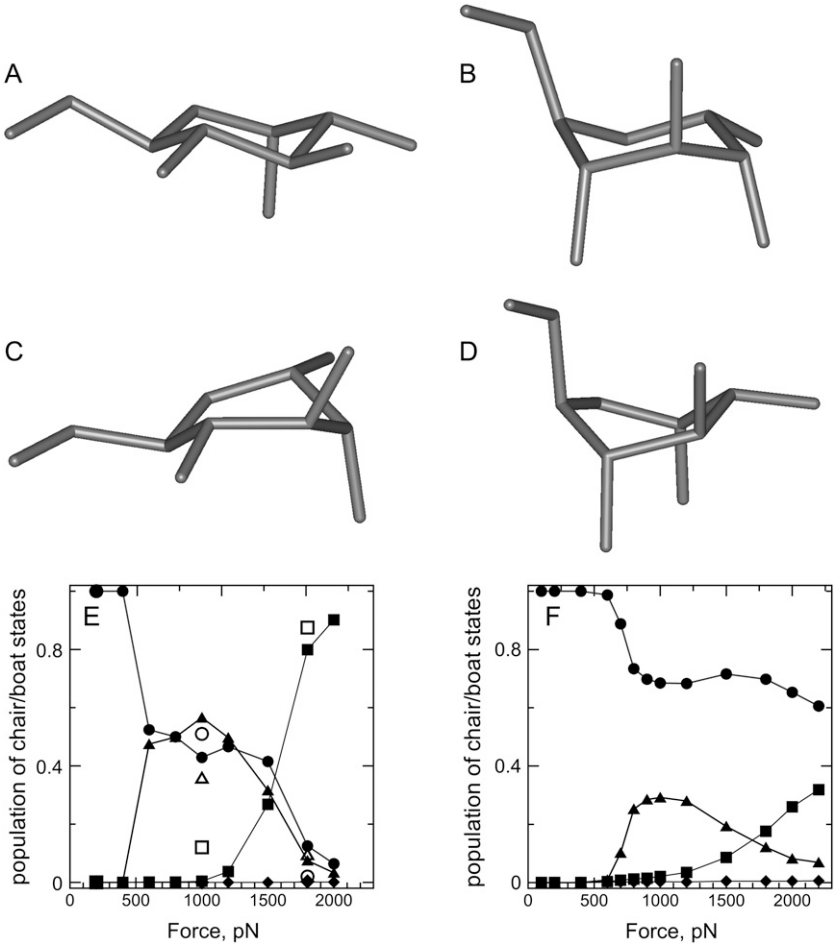

FIGURE 6 Conformations of dextran monomer during extension. (*A*) chair ($^4C_1$), (*B*) inverted chair ($^1C_4$), (*C*) boat, and (*D*) inverted boat. Boat conformations extracted from simulation are actually a mixture of boat and twisted boat conformations. (*E*,*F*) Population of glucopyranose ring conformation states: chair ($^4C_1$) (*circles*), inverted chair ($^1C_4$) (*triangles*), boatlike (*squares*), and inverted boatlike (*diamonds*) conformations for inner dextran monomers in 10-mer: (*E*) AMBER94 and (*F*) AMBER-GLYCAM04 force fields at T = 300 K.

State 2: If $\phi 1 \geq 0$ and $\phi 2 \leq 0$, the ring is in inverted chair conformation.
State 3: If $\phi 1 > 0$ and $\phi 2 > 0$, the ring is in boat conformation.
State 4: If $\phi 1 < 0$ and $\phi 2 < 0$, the ring is in inverted boat conformation.

The last conformation was almost absent in all simulations but it is considered for completeness. This definition of four ''main'' conformations of glucopyranose ring is rather rough, as it does not discriminate between all possible conformations but only between four main groups of conformations. But it is reasonable because from Fig. 4 for theC2C1O5C5 and C2C3C4C5 dihedral angles we have seen that population of these pairs is nonzero only at three compact areas around 1), ($\phi 1$, $\phi 2$) = ($-60°$, $60°$); 2), ($\phi 1$, $\phi 2$) = ($60°$, $-60°$); and 3), ($\phi 1$, $\phi 2$) = ($30°$, $30°$) corresponding to chair, inverted chair, and boat conformations.

To extract the probability of each of these four states, the number of conformations in each state was normalized by the total number of glucopyranose ring states occurring during entire simulation. The results are shown on Fig. 6, *F* and *G*, for 10-mer as a function of external force. The qualitative behavior of the populations of states of glucopyranose ring for AMBER94 (Fig. 6 *E*) and for AMBER-GLYCAM04 (Fig. 6 *F*) force fields at $T = 300$ K is similar. The chair ($^4C_1$) conformation state of the ring is dominant at low force and its population decreases with force. The number of boat conformations increases with force and become dominant at high force. The inverted chair conformation for both force fields occurs first at F = 600 pN and its population peak is at forces 800–1200 pN.

Comparison of populations of the same states for AMBER-GLYCAM04 with CHARMM monomers at $T = 300$ K (not shown) reveals that for the CHARMM force field there is no inverted chair conformation ($^1C_4$) and only an abrupt transition from the chair ($^4C_1$) conformation to boat occurs at forces near 1000 pN.

Thus the main result both for AMBER94 and AMBER-GLYCAM04 is that, in the plateau region, only transitions from chair to inverted chair (i.e., from $^4C_1$ to $^1C_4$) occur. Transitions to a boat conformation occur mainly at higher forces ($F > 1500$ pN). This suggests that in the experimental plateau region (F = 700–1000 pN), the glucopyranose conformational transitions occur only from chair to inverted chair. As transitions to the boat conformation occur at forces $F > 1500$ pN they could not contribute significantly to the occurrence of the plateau in the experimentally observed range.

This result means that despite the existence of three main states (chair, inverted chair, and boat) of the glucopyranose rings over the experimental interval of force (200–2000 pN) of single molecule dextran extension in AFM, a more coarse-grained two-state model (such as a model of chain consisting of bistable bonds (28)) may be sufficient for the theoretical description of the plateau on force-extension curve because only one process contributes to the transition in plateau region. However, our simulations using AMBER-type force fields lead to the interpretation of this process as a chair to inverted chair transition of ring as opposed to chair-boat transition proposed in previous CHARMM-based simulations.

Dextran 10-mer in explicit water

We performed simulations of dextran 10-mer in explicit water solvent at three different forces (F = 200, 1000, and 1800 pN), i.e., before, around, and after the plateau region on the force-extension curve. For each monomer of the 10-mer, the monomer length and dihedral angles reflecting the rotation around the C5-C6 bond and the puckering behavior of the pyranose ring were analyzed.

The average monomer length at $F = 200$ pN (not shown) is near $d = 5.2$ Å, which is close to the value for the $^4C_1$ conformation of the pyranose ring obtained at this force in vacuo for both the dextran monomer and the 10-mer. As, in vacuo, the *gt* substate of $^4C_1$ conformation is less probable than $g-g$ and $tg-$ even at this smallest force used (200 pN). At intermediate extensions (F = 1000 pN corresponding to plateau in the force-extension curve) the distribution of monomer length of 10-mer in water is bimodal (not shown) with a first peak at $d \approx 5.5$ Å and a second broad peak at $d \approx$ 5.9 Å. These two monomer lengths are close to those we obtained in vacuo and correspond to a slightly extended $^4C_1$ ($g-g$ or $tg-$) chair and $^1C_4$ ($tg-$) inverted chair. At the highest force ($F = 1800$ pN), the monomer length is close to $d \approx 6.2$ Å. This length of monomer is also very close to the monomer length obtained for the 10-mer in vacuo with pyranose rings in a boat/twisted boat conformation.

The values of pairs of dihedral angles O5C5C6O6 and C4C5C6O6 reflecting rotation around C5-C6 bond and angles C2C1O5C5 and C2C3C4C5 reflecting conformational transitions of the glucopyranose ring are slightly different from the values obtained in vacuo but distributed (not shown) between the same three compact areas as in Fig. 4. The signs of the latter pair of angles were used to determine the population of the chair, inverted chair, and boat states of the glucopyranose rings of a 10-mer in water at F = 200, 1000, and 1800 pN (*open points* in Fig. 6 *E*). At $F = 200$ pN all glucopyranose rings are in the chair conformation; at F = 1000 pN there is near 58% chair, 35% inverted chair, and <10% boat conformations; at highest force ($F = 1800$ pN) there is almost no chair conformation, near 10% of inverted chair, and near 90% boat/twisted boat conformation. These data are in good agreement with results obtained for the same AMBER94 force field in the absence of water (Fig. 6 *E*). At the same time, we can also make the preliminary conclusion that the explicit water solvent at F = 1000 pN decreases the amount of inverted chair conformations and slightly increases the amount of boat conformations in comparison with similar simulation in vacuo.

CONCLUSIONS

The equilibrium structural properties of dextran under force have been determined using molecular dynamics with three different force fields (AMBER94, AMBER-GLYCAM04, and CHARMM), in vacuo. The main result is that, at forces between 700 and 1000 pN, a third state of the glucopyranose ring (inverted chair) not previously described for dextran is observed beside chair and boat. Remarkably, the plateau on the force-extension profile from both simulations and experiments can be explained by the transition of the glucopyranose ring from chair ($^4C_1$) to inverted chair ($^1C_4$).

Other processes occur at smaller (rotation around the C5C6 bond) or higher (chair to boat transition) forces. These results are observed with two different AMBER-based force fields. For CHARMM at $T = 300$ K, no inverted chair ($^1C_4$) conformation of the pyranose ring are observed. However, at $T = 600$ K, CHARMM behaves similarly to AMBER-based force fields, suggesting that CHARMM might possibly overestimate the height of the barrier between stable states.

Thus, at room temperature, AMBER-based and CHARMM force fields suggest different molecular mechanisms for the plateau region in the force-extension curve: AMBER94 and AMBER-GLYCAM04 associate the plateau to the chair-inverted chair transition while CHARMM assigns the plateau region to chair-boat transitions.

Simulations in explicit water of dextran 10-mer extension confirm that the results above are not an artifact due to the absence of solvation.

The subtle forms of the transitions of dextran under load that we have identified in this work immediately motivate a number of challenges for the experimentalists. Firstly, the three-state nature of the monomeric length increase in the range of 1000–2000 pN should be observable even in standard force spectroscopy with careful control of signal to noise. In fact, while previous experiments never reported a three-state mechanism, very recent experimental work (31) has suggested a three-state structure to the dextran extensional transition compatible with our findings. Using a novel AFM approach based on the analysis of the variance of the extension an intermediate was detected for a single dextran molecule compatible with the intermediate conformation of the glucopyranose ring revealed by our simulations. Furthermore, the simulations suggest that a one-dimensional reaction coordinate could not be an appropriate low-dimensional description of the transition landscape. The two chair states are well-separated along the predominant axis of extension, but the boat state, which acts as a transition state between them at low force and a basin of attraction at high force, is, as we have seen, almost orthogonal to the extensional axis, contributing much less to the extension of the monomer. A minimal projection of the landscape would therefore be two-dimensional, corresponding to the two conformational angles that reflect the three states. Experimental techniques that are sensitive to such structures in transition landscapes are being developed. These include extensions of force spectroscopy that themselves access more than one degree of freedom as a function of extension or force, and so are in principle capable of mapping out the structure of configuration spaces with an equal number of degrees of freedom (28,32). In particular, one consequence of this two-dimensional model for dextran is that the transition state between the basins for chair and inverted chair would appear to be very sharp when projected onto the direction of extension. Experiments that are sensitive to the rate dependence of conformational transitions should be able to detect this feature.

We thank Steve Homans, Peter Olmsted, and Bhavin Khatri for interesting discussions and F. A. Momany for communication of unpublished data.

This work was supported by Engineering and Physical Sciences Research Council, grants No. GR/S67388/01 and No. EP/C528336/1. E.P. thanks International Association for the Promotion of Cooperation with Scientists from the New Independent States from the former Soviet Union for partial financial support (grant No. 05-1000004-7747).

REFERENCES

1. Rief, M., F. Oesterhelt, B. Heymann, and H. E. Gaub. 1997. Single molecule force spectroscopy on polysaccharides by atomic force microscopy. *Science*. 275:1295–1297.
2. Marszalek, P. E., A. F. Oberhauser, Y. P. Pang, and J. M. Fernandez. 1998. Polysaccharide elasticity governed by chair-boat transitions of the glucopyranose ring. *Nature*. 396:661–664.
3. Marszalek, P. E., Y. P. Pang, H. B. Li, J. El Yazal, A. F. Oberhauser, and J. M. Fernandez. 1999. Atomic levers control pyranose ring conformations. *Proc. Natl. Acad. Sci. USA*. 96:7894–7898.
4. Fisher, T. E., P. E. Marszalek, A. F. Oberhauser, M. Carrion-Vazquez, and J. M. Fernandez. 1999. The micro-mechanics of single molecules studied with atomic force microscopy. *J. Physiol.* (*London.*) 520:5–14.
5. Lee, G., W. Nowak, J. Jaroniec, Q. M. Zhang, and P. E. Marszalek. 2004. Molecular dynamics simulations of forced conformational transitions in 1,6-linked polysaccharides. *Biophys. J.* 87:1456–1465.
6. Kuttel, M., J. W. Brady, and K. J. Naidoo. 2002. Carbohydrate solution simulations: producing a force field with experimentally consistent primary alcohol rotational frequencies and populations. *J. Comput. Chem.* 23:1236–1243.
7. Melberg, S., K. Rasmussen, R. Scordamaglia, and C. Tosi. 1979. Nonbonded interactions in *d*-glucose and β-maltose—ab initio study of conformations produced by empirical force-field calculations. *Carbohydr. Res.* 76:23–37.
8. Cramer, C. J., and D. G. Truhlar. 1993. Quantum-chemical conformational analysis of glucose in aqueous solution. *J. Am. Chem. Soc.* 115:5745–5753.
9. Barrows, S. E., C. J. Cramer, F. J. Dulles, A. D. French, and D. G. Truhlar. 1995. Quantum chemical conformational analysis of glucose in the gas phase and in solution. *Abstr. Papers Am. Chem. Soc.* 209:111.
10. Appell, M., G. Strati, J. L. Willett, and F. A. Momany. 2004. B3LYP/6–311^{++}G** study of α- and β-*d*-glucopyranose and 1,5-anhydro-*d*-glucitol: C–4(1) and C–1(4) chairs, B–3,B–O and B–3,B–0 boats, and skew-boat conformations. *Carbohydr. Res.* 339:537–551.
11. Weiner, S. J., P. A. Kollman, D. T. Nguyen, and D. A. Case. 1986. An all-atom force field for simulations of proteins and nucleic acids. *J. Comput. Chem.* 7:230–252.
12. MacKerell, A. D., D. Bashford, M. Bellott, R. L. Dunbrack, J. D. Evanseck, M. J. Field, S. Fischer, J. Gao, H. Guo, S. Ha, D. Joseph-McCarthy, L. Kuchnir, K. Kuczera, F. T. K. Lau, C. Mattos, S. Michnick, T. Ngo, D. T. Nguyen, B. Prodhom, W. E. Reiher, B. Roux, M. Schlenkrich, J. C. Smith, R. Stote, J. Straub, M. Watanabe,

J. Wiorkiewicz-Kuczera, D. Yin, and M. Karplus. 1998. All-atom empirical potential for molecular modeling and dynamics studies of proteins. *J. Phys. Chem. B.* 102:3586–3616.

13. Dowd, M. K., A. D. French, and P. J. Reilly. 1994. Modeling of aldopyranosyl ring puckering with MM3(92). *Carbohydr. Res.* 264:1–19.
14. Senderowitz, H., C. Parish, and W. C. Still. 1996. Carbohydrates: united atom AMBER* parameterization of pyranoses and simulations yielding anomeric free energies. *J. Am. Chem. Soc.* 118:8985.
15. Homans, S. W. 1990. A molecular mechanical force-field for the conformational-analysis of oligosaccharides—comparison of theoretical and crystal-structures of MAN-α-1–3MAN-β-1–4GLCNAC. *Biochemistry.* 29:9110–9118.
16. Woods, R. J., R. A. Dwek, C. J. Edge, and B. Fraserreid. 1995. Molecular mechanical and molecular dynamical simulations of glycoproteins and oligosaccharides. 1. GLYCAM-93 parameter development. *J. Phys. Chem.* 99:3832–3846.
17. Senderowitz, H., and W. C. Still. 1997. A quantum mechanically derived all-atom force field for pyranose oligosaccharides. AMBER parameters and free energy simulations. *J. Org. Chem.* 62:1427–1438.
18. Eklund, R., and G. Widmalm. 2003. Molecular dynamics simulations of an oligosaccharide using a force field modified for carbohydrates. *Carbohydr. Res.* 338:393–398.
19. Kirschner, K. N., and R. J. Woods. 2001. Solvent interactions determine carbohydrate conformation. *Proc. Natl. Acad. Sci. USA.* 98:10541–10545.
20. Leroux, B., H. Bizot, J. W. Brady, and V. Tran. 1997. Water structuring around complex solutes: theoretical modeling of α-*d*-glucopyranose. *Chem. Phys.* 216:349–363.
21. Hemmingsen, L., D. E. Madsen, A. L. Esbensen, L. Olsen, and S. B. Engelsen. 2004. Evaluation of carbohydrate molecular mechanical force fields by quantum mechanical calculations. *Carbohydr. Res.* 339:937–948.
22. Cornell, W. D., P. Cieplak, C. I. Bayly, I. R. Gould, K. M. Merz, D. M. Ferguson, D. C. Spellmeyer, T. Fox, J. W. Caldwell, and P. A. Kollman. 1995. A second generation force field for the simulation of proteins, nucleic acids, and organic molecules. *J. Am. Chem. Soc.* 117:5179–5197.
23. Melberg, S., and K. Rasmussen. 1980. Conformations of disaccharides by empirical, force-field calculations. 3. β-gentiobiose. *Carbohydr. Res.* 78:215–224.
24. Best, R. B., G. E. Jackson, and K. J. Naidoo. 2001. Molecular dynamics and NMR study of the $\alpha(1 \rightarrow 4)$ and α $(1 \rightarrow 6)$ glycosidic linkages: maltose and isomaltose. *J. Phys. Chem. B.* 105:4742–4751.
25. Bernardi, A., A. Colombo, and I. Sanchez-Medina. 2004. Conformational analysis and dynamics of mannobiosides and mannotriosides using Monte Carlo/stochastic dynamics simulations. *Carbohydr. Res.* 339:967–973.
26. Corzana, F., M. S. Motawia, C. H. Du Penhoat, S. Perez, S. M. Tschampel, R. J. Woods, and S. B. Engelsen. 2004. A hydration study of $(1 \rightarrow 4)$ and $(1 \rightarrow 6)$ linked α-glucans by comparative 10 ns molecular dynamics simulations and 500-MHz NMR. *J. Comput. Chem.* 25:573–586.
27. Rabinovich, A. L., P. O. Ripatti, N. K. Balabaev, and F. A. M. Leermakers. 2003. Molecular dynamics simulations of hydrated unsaturated lipid bilayers in the liquid-crystal phase and comparison to self-consistent field modeling. *Phys. Rev. E.* 67:011909.
28. Kawakami, M., K. Byrne, B. Khatri, T. C. B. McLeish, S. E. Radford, and D. A. Smith. 2004. Viscoelastic properties of single polysaccharide molecules determined by analysis of thermally driven oscillations of an atomic force microscope cantilever. *Langmuir.* 20:9299–9303.
29. Berendsen, H. J. C., J. P. M. Postma, W. F. Vangunsteren, A. Dinola, and J. R. Haak. 1984. Molecular-dynamics with coupling to an external bath. *J. Chem. Phys.* 81:3684–3690.
30. Cremer, D., and J. A. Pople. 1975. General definition of ring puckering coordinates. *J. Am. Chem. Soc.* 97:1354–1358.
31. Walther, K. A., J. Brujic, H. B. Li, and J. M. Fernandez. 2005. Fluctuation analysis of single dextran molecules observed with force-clamp spectroscopy. *Biophys. J.* 88:170A.
32. Kawakami, M., K. Byrne, B. S. Khatri, T. C. B. McLeish, S. E. Radford, and D. A. Smith. 2005. Viscoelastic measurements of single molecules on a millisecond time scale by magnetically driven oscillation of an atomic force microscope cantilever. *Langmuir.* 21:4765–4772.
33. Fernandez, J. M., M. Carrion-Vasquez, H. Li, A. Oberhauser, and P. Marszalek. 2002. Stretching single molecules into novel conformations using the atomic force microscope. *Abstr. Papers Am. Chem. Soc.* 223:C30–C31.